analytical chemistry

pubs.acs.org/ac Article

Aptamer-Based Field-Effect Transistor for Detection of Avian Influenza Virus in Chicken Serum

Jae Kwon,[§] Yeonju Lee,[§] Taek Lee,* and Jae-Hyuk Ahn*

Cite This: *Anal. Chem.* 2020, 92, 5524−5531 Read Online

ACCESS | Metrics & More | Article Recommendations | Supporting Information

ABSTRACT: Early diagnosis of the highly pathogenic H5N1 avian influenza virus (AIV) is significant for preventing and controlling a global pandemic. However, there is no existing electrical biosensor for detecting biomarkers for AIV in clinically relevant samples such as chicken serum. Herein, we report the first use of an aptamer-functionalized field-effect transistor (FET) as a label-free sensor for AIV detection in chicken serum. A DNA aptamer is employed as a sensitive and selective receptor for hemagglutinin (HA) protein, which is a biomarker for AIVs. This aptamer is immobilized on a gold microelectrode that is connected to the gate of a reusable FET transducer. The specific binding of the target protein results in a change in the surface potential, which generates a signal response of the FET transducer. We hypothesize that a conformational change in the DNA aptamer upon specific binding of HA protein may alter the surface potential. The signal of the aptamer-based FET biosensor increased linearly with the increase in the logarithm of HA protein concentration in a dynamic range of 10 pM to 10 nM with a detection limit of 5.9 pM. The selectivity of the biosensor for HA protein was confirmed by employing relevant interfering proteins. The proposed biosensor was successfully applied to the selective detection of HA protein in a chicken serum sample. Owing to its simple and low-cost architecture, portability, and sensitivity, the aptamer-based FET biosensor has potential as a point-of-care diagnosis of H5N1 AIVs in clinical samples.

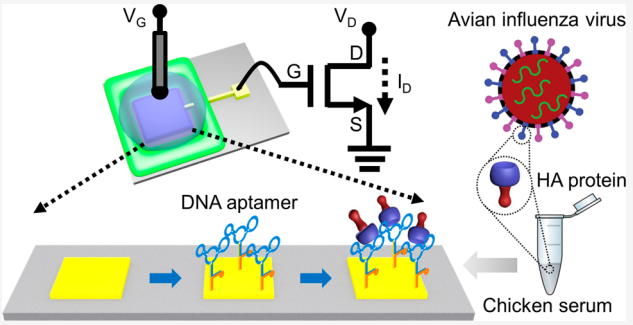

Avian influenza viruses (AIVs) pose a crucial threat to the poultry industry and public health. The highly pathogenic H5N1 AIV causes severe disease in poultry with almost 100% mortality rate.[1] It can cross the species barrier and infect humans directly. The first human infection caused by H5N1 was reported in Hong Kong in 1997, with 18 cases and 6 deaths.[2−4] The World Health Organization has reported 861 human cases of H5N1 infection, including 455 deaths, since 2003.[5] This virus can easily spread from person to person and thus lead to a global pandemic. Therefore, rapid detection and prevention of H5N1 AIV are required to control its outbreak.

Conventional methods for detecting H5N1 AIV include virus isolation culture,[2,3] identification of influenza-specific RNA by reverse-transcription polymerase chain reaction,[6] and direct antigen detection by enzyme-linked immunosorbent assay.[7] These methods are generally effective but require time-consuming procedures, bulky and expensive equipment, and trained technicians, which limits their applications in on-site use. As an alternative, label-free electrical detection of H5N1 AIV based on field-effect transistors (FETs) is suitable for portable applications in field tests because it provides rapid signal response, hand-held readout system, low cost, and easy operation.[8−10] An FET is greatly advantageous for a transducer because it offers superior limit of detection, which is as low as the picomolar level, analysis of a small sample volume, and scalable manufacturing process.[11−13]

Besides transducers, appropriate selection of bioreceptors is also critical to achieve high performance. DNA aptamers, which are artificial DNA segments that bind to a specific target molecule, are considered a suitable bioreceptor for the detection of H5N1 AIVs.[14] Compared with antibodies, DNA aptamers have advantages in on-site use in terms of high chemical stability, low production cost, easy chemical modification, tunable binding affinity, and reproducibility.[15] DNA aptamers targeting H5N1 AIVs have been applied for other types of transducers, such as fluorescence,[16,17] surface plasmon resonance,[18,19] impedance,[20,21] and electrochemistry.[22,23] However, there is a lack of research on H5N1 AIV detection using an aptamer-based FET biosensor and its working principle, even though the concept and applications of aptamer-functionalized FETs in biosensing have been studied.[24−29] Moreover, there is no existing FET-based biosensor for the detection of H5N1 AIVs in clinically relevant samples such as chicken serum.

Received: January 22, 2020
Accepted: March 9, 2020
Published: March 9, 2020

https://dx.doi.org/10.1021/acs.analchem.0c00348
Anal. Chem. 2020, 92, 5524−5531

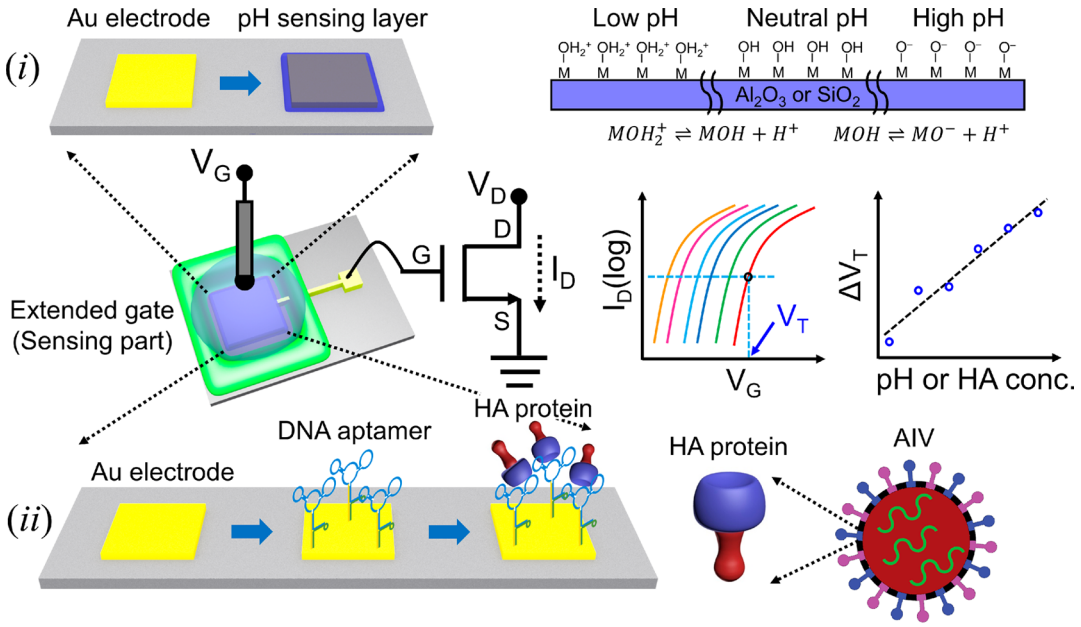

Figure 1. Schematic of the extended-gate FET for (i) pH sensing and (ii) AIV detection. For pH sensing, the Au electrode of a sensing part (i.e., extended gate) is modified with a pH-sensitive dielectric (i.e., Al_2O_3 or SiO_2). Hydrogen ions are reversibly bound on active sites of the dielectric, and the surface charge results in the surface potential depending on the pH value. For AIV detection, the Au electrode of the sensing part is functionalized with DNA aptamer specific to HA protein, which is displayed on the AIV and used as a target protein. Surface potential is generated due to a conformational change in DNA aptamer induced by the binding of HA protein. In both experiments, the generated surface potential is transferred with an FET transducer by connecting the sensing part to the gate of the FET transducer, where the drain current (I_D) is measured as a function of the gate voltage (V_G) applied with a reference electrode inserted into the target solution. The surface potential shifts the transfer characteristics (I_D−V_G) and modulates the threshold voltage (V_T), defined as a gate voltage to flow the certain drain current. V_T, as a sensing signal in this study, is dependent on the pH and concentration of HA protein.

This is the first paper to report on the FET-based detection of H5N1 AIVs by using DNA aptamer as a bioreceptor. The DNA aptamer was designed to capture hemagglutinin (HA) protein, a glycoprotein found on the AIV surface. The DNA aptamer was functionalized on a sensing part (i.e., extended gate) of the FET transducer, and the specific binding with HA proteins resulted in a change in the electrical characteristics of the FET transducer. Our aptamer-based FET sensor could detect HA proteins at picomolar levels in both buffer solution and chicken serum. We investigated the specificity of the DNA aptamer by measuring the signals from other interfering proteins. Our analysis of the electrical characteristics of the FET provided the transduction mechanism based on a conformational change in the DNA aptamer, induced by binding of HA protein. In addition, the detection ability for charged biomolecules was confirmed through pH-sensing experiments. Figure 1 shows a schematic of our aptamer-based FET sensor and the experimental procedure.

EXPERIMENTAL SECTION

Materials. To test the device as a charge sensor, pH buffer solutions (pH 3−11) were purchased from Samchun Pure Chemical Co., Ltd. (South Korea).

The influenza A H5N1 (A/VietNam/1203/2004) Hemagglutinin/HA Protein (His & Fc Tag), which is the target for H5N1 AIV detection, was purchased from Sino Biology (China). The specific DNA aptamer against the HA protein contained the sequence of 5′-GTG TGC ATG GAT AGC ACG TAA CGG TGT AGT AGA TAC GTG CGG GTA GGA AGA AAG GGA AAT AGT TGT CCT GTT GTT GCC ATG TGT ATG TGG G-3′.[23,30] To form covalent bonds with the gold electrode using a thiol group, the DNA aptamer was hybridized with thiol-tagged DNA oligonucleotide (SH-5′-GGA TCA ATC ATG G CA A-3′). The DNA aptamer was also hybridized with HRPzyme-tagged DNA oligonucleotide (5′-TTT GGG TAG GGC GGG TTG GGC CCA CAT ACT TTG TTG ATC C-3′) to create the DNA 3 way-junction (3WJ). All DNA sequences were synthesized by Bioneer (South Korea). The predicted multifunctional DNA structure was described in our previous study.[23] Hemoglobin, bovine serum albumin (BSA), and myoglobin for a selectivity test were purchased from Sigma-Aldrich (United States). For a clinical trial, a chicken serum was purchased from Thermo Fisher Scientific (United States) and the HA protein was dissolved with 10% chicken serum. A phosphate-buffered saline (PBS) solution (pH 7.4) was purchased from Fisher Scientific (United States).

Fabrication of Sensing Electrode. Sensing electrodes with metal layers (Cr/Au = 3 nm/100 nm) were fabricated on a 4-in silicon wafer with a 90 nm-thick layer of SiO_2 via conventional semiconductor processes including photolithography, electron-beam evaporation, and lift-off process. The fabricated wafer was then diced into small pieces (1 × 0.8 cm). The dimension of the sensing electrode was 2 × 2 mm or 3 × 3 mm.

For the pH sensing experiment, a pH-sensitive dielectric (Al_2O_3 or SiO_2) with a thickness of 15 nm were deposited on the sensing electrode by electron-beam deposition. No additional modification of the sensing electrode was performed for the detection of HA proteins, because thiol linkers in DNA aptamers can bind on the Au surface of the sensing electrode. A reservoir for storing the test solutions was constructed using a silicone elastomer (Kwik-Cast, World Precision Instruments, Inc.). Representative optical microscopy images of the

https://dx.doi.org/10.1021/acs.analchem.0c00348
Anal. Chem. 2020, 92, 5524−5531

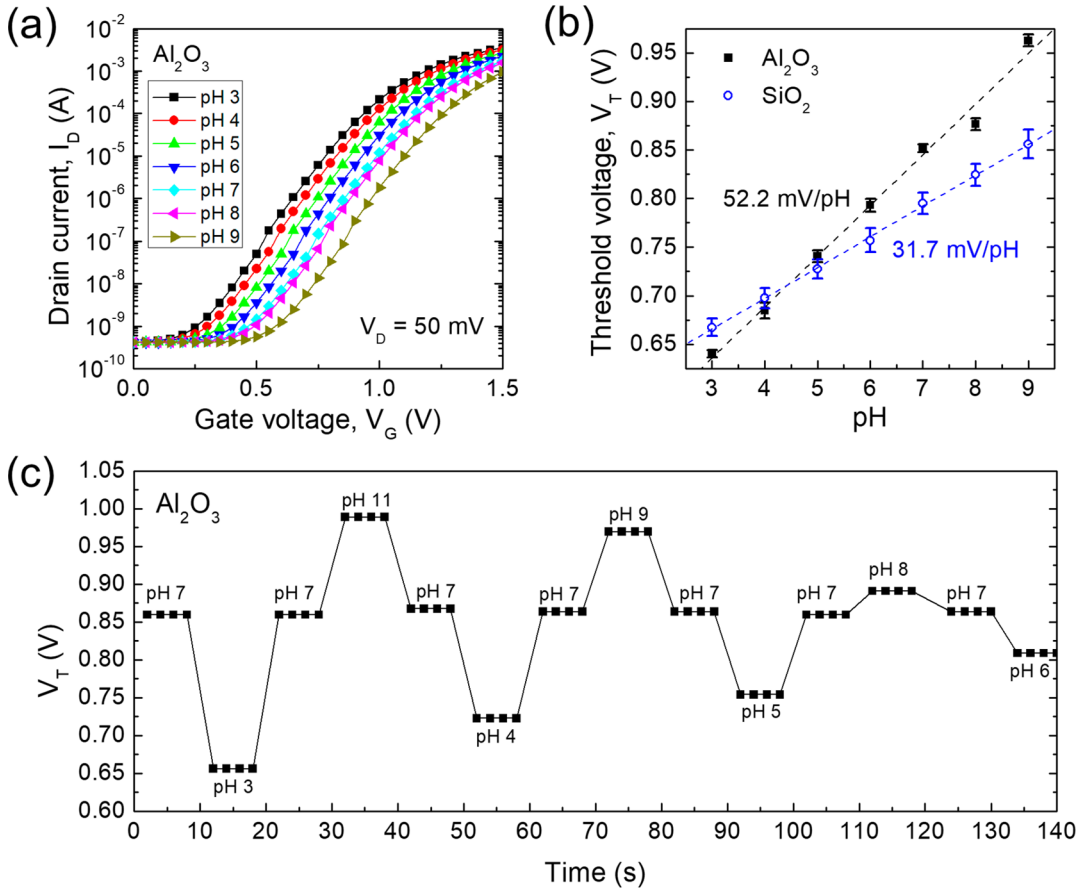

Figure 2. pH sensing characteristics of the extended-gate FET with pH-sensitive dielectrics deposited on the sensing electrode. (a) I_D−V_G characteristics of Al_2O_3-depoisted extended-gate FET as a function of pH. (b) V_T of the extended-gate FET versus pH. A higher pH sensitivity is observed in the Al_2O_3 layer compared to the SiO_2 layer. (c) Time-resolved pH measurement with the Al_2O_3 sensing layer. The sensitive and stable pH sensing results as a proof-of-concept confirm the biosensing ability of the extended-gate FET by detecting a change in the surface potential.

fabricated sensing electrodes are provided in Supporting Information (Figure S1).

Immobilization Method. The three fragments of DNA 3WJ were assembled into one unit by an annealing process through heating at 80 °C for 5 min, followed by cooling down to 4 °C at a rate of 4 °C/min using a Thermal Cycler (Biorad, United States). The assembled DNA aptamer was confirmed by native-tris boric acid magnesium polyacrylamide gel electrophoresis in our previous study.[23] A 3 μL drop of the assembled DNA aptamer (1 μM) was cast on the sensing electrode for 3 h, followed by cleaning with deionized water to remove the unreacted DNA aptamers and then drying with nitrogen gas. The sensing electrode was then incubated with a 3 μL drop of PBS buffer or chicken serum containing the target HA protein for 2 h, followed by rinsing with deionized water to clean the unbound HA protein and drying with nitrogen gas.

Surface Morphology Investigation by Atomic Surface Microscopy. The surface of the sensing electrode (i.e., Au surface) after each functionalization with the DNA aptamer and HA protein was investigated by atomic surface microscopy (AFM) in the tapping mode (Nanoscope IV/Multimode, Digital Instruments, United States). A phosphorus-doped silicon probe (RTESP, Bruker, United States) was employed for imaging of samples within a 1 × 1 μm scanning area. The surface roughness and vertical distance of the Au electrodes were obtained after each functionalization. The surface roughness and vertical distance of each image were obtained using the NanoScope software. The root-mean-square roughness (R_q), maximum height (R_{max}), and roughness average (R_a) indicate the standard deviation of height, highest peak of the surface, and absolute value of the height of the surface profile, respectively.

Electrical Characterization. A commercially available n-type MOSFET (2SK3018T106, ROHM) was utilized as a readout transistor (i.e., FET transducer) to convert the surface potential on the sensing electrode to the drain current. The sensing electrode was connected to the gate terminal of the FET transducer. A test solution was placed on the sensing electrode, and then, an Ag/AgCl reference electrode (MF-2052, Bioanalytical Systems, Inc.) was immersed into the solution. The transfer characteristics of the extended-gate FETs were measured with a SourceMeter (Keithley 2614B). The drain current under a drain voltage of 50 mV was measured while the gate voltage applied to the reference electrode was swept from −0.35 to 2 V and the source terminal was electrically grounded.

The threshold voltage (V_T) is a sensing signal, which is defined as a gate voltage for the flow of the drain current of 1 μA in the subthreshold region. This constant-current method can reduce the effect of the parasitic resistance; this leads to less noise in the extraction of V_T as compared to the extrapolation method.[31]

The limit of detection (LOD) was calculated according to the equation LOD = $\frac{3.3\sigma}{S}$, where σ is the standard deviation of

https://dx.doi.org/10.1021/acs.analchem.0c00348
Anal. Chem. 2020, 92, 5524−5531

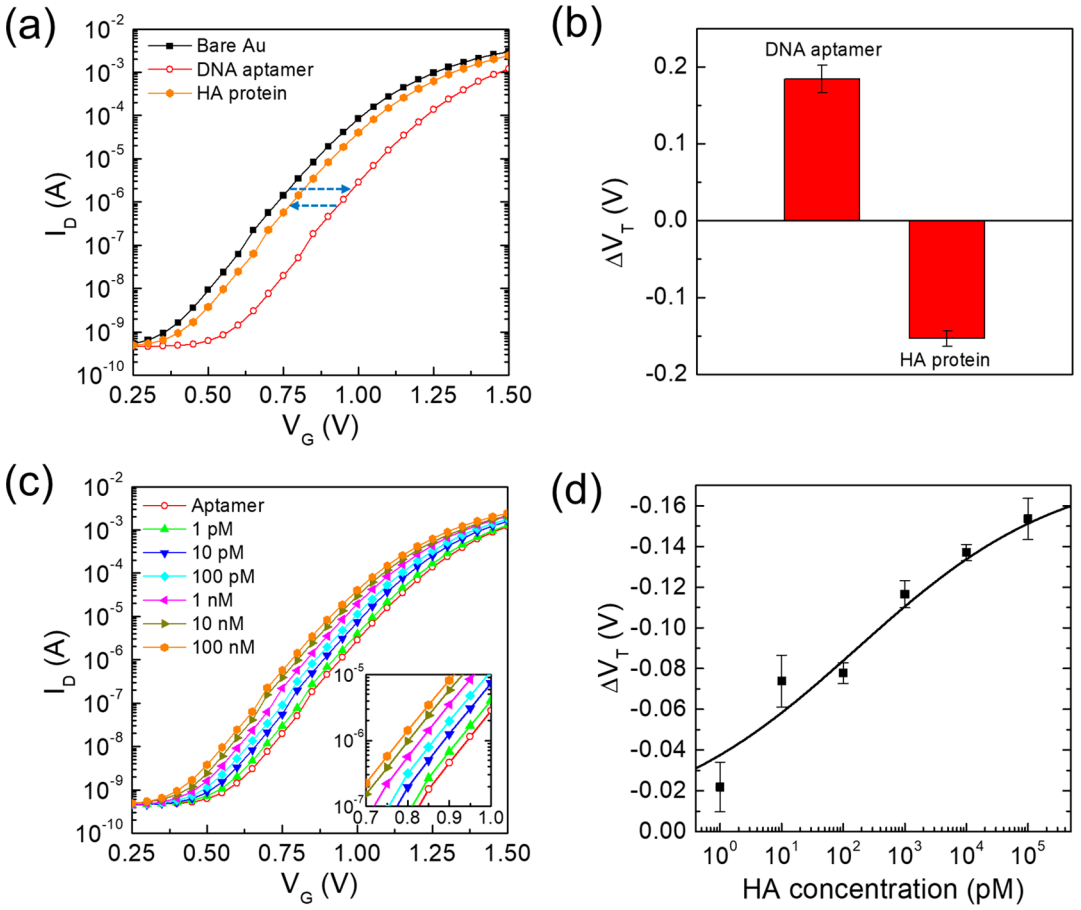

Figure 3. Detection of HA protein in a buffer solution. (a) I_D−V_G characteristics of the extended-gate FET with no surface treatment (bare Au), immobilization of DNA aptamer on the Au electrode (DNA aptamer), and binding of HA protein on the DNA aptamer-functionalized electrode (HA protein). (b) V_T shift caused by the DNA aptamer and HA protein. The opposite direction of the V_T shifts indicates the opposite polarity of the surface potentials generated by the DNA aptamer and HA protein. (c) I_D−V_G characteristics and (d) V_T shift of the aptamer-immobilized extended-gate FET with different concentrations of HA protein dissolved in a buffer solution. The measured data are fit to the Sips model (solid line).

the response (or the standard deviation of *y*-intercepts of regression lines) and *S* is the slope of the calibration curve.[32] The calibration curves were produced using $N > 3$ samples within a dynamic range.

To increase the sensing signal using low ionic strength,[33] 0.1 × PBS and 0.001 × PBS were used as measurement buffers for detecting HA protein in purified buffer and chicken serum, respectively. The effect of Debye screening is discussed in the Results and Discussion.

RESULTS AND DISCUSSION

pH Sensing Characteristics. As a well-known proof-of-concept example for confirming the detection ability of the proposed sensor for charged biomolecules, we conducted a pH sensing experiment by modifying the sensing electrode with a pH-sensitive dielectric (i.e., Al_2O_3 or SiO_2). As the pH value decreased, the drain current (I_D) versus gate voltage (V_G) shifted to the left in the Al_2O_3-deposited device (Figure 2a). Similar shifts of the curve by the pH value were observed for the SiO_2-coated device (Figure S2). The sensing mechanism is based on the site-binding model,[34,35] where active sites are derived on the sensing dielectrics to capture and release hydrogen ions (Figure 1). At a lower pH value, a relatively large number of positively charged hydrogen ions in the buffer solution were bound on the active sites of the dielectric, and thus, generated positive surface potential, resulting in a decrease in the threshold voltage, V_T. In contrast, positively charged hydrogen ions were detached from the active sites at a higher pH value and the surface potential was reduced. Figures 2b and c show that V_T, as the sensing signal, is linearly dependent on the pH value on both Al_2O_3 and SiO_2 surfaces with high reproducibility. This proof-of-concept experiment indicates that our extended-gate biosensor can sense a change in the surface charge and detect the charged species, particularly HA proteins in this study.

The device with the Al_2O_3 layer exhibited a pH sensitivity higher than that with the SiO_2 layer. The difference in the sensing signal at the same pH value (i.e., the same concentration of hydrogen ions) indicates that the sensitivity depends on the choice of the sensing material. For maximizing detection sensitivity in biosensing, the choice of receptor and its immobilization method should be considered.

Surface Characterization. An analysis of surface roughness and vertical distance extracted from AFM images confirmed the immobilization of the DNA aptamer and HA protein on the Au electrode. The values of surface roughness (R_q) were 0.492, 0.948, and 2.245 nm and those of the vertical distance were 1.797, 3.482, and 6.127 nm for the bare Au electrode, DNA aptamer, and HA protein, respectively (Figure S3). The increased values of both the surface roughness and

https://dx.doi.org/10.1021/acs.analchem.0c00348
Anal. Chem. 2020, 92, 5524−5531

Table I. Comparison of Previously Reported FET-Based Sensors for AIV Detection

solution	bioreceptor	target	FET-type	LOD	dynamic range	reference
chicken serum	DNA aptamer	HA protein	extended gate	5.9 pM	10 pM−10 nM	this work
cloacal swab	antibody	nucleoprotein	extended gate	10^3 EID_{50} mL^{-1}	10^2−10^5 EID_{50} mL^{-1}	10
1× PBS	antigen	antibody	silicon nanowire	1 nM	N/A	8
1× PBS	DNA probe	DNA target	reduced graphene oxide	50 pM	10 pM−100 nM	43
0.1× PBS	DNA probe	DNA target	silicon nanowire	1 fM	1 fM−10 pM	41
0.01× PBS	glycan	HA protein	ion-sensitive Si-FET	few aM	500 zM−500 pM	42

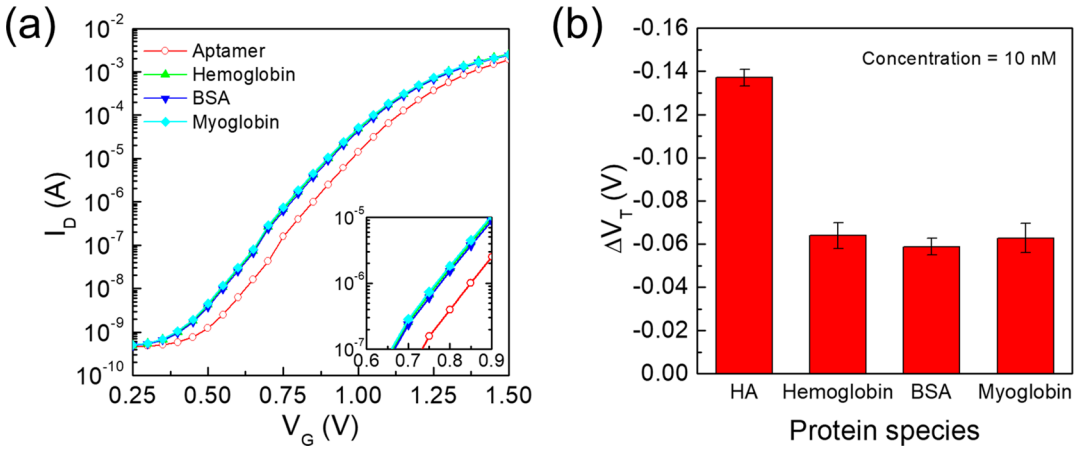

Figure 4. Selectivity of the extended-gate FET after functionalization of DNA aptamer for interfering proteins. (a) I_D−V_G characteristics and (b) V_T shift by various proteins (hemoglobin, BSA, and myoglobin).

vertical distance confirmed a proper modification of the Au electrode with the DNA aptamer and subsequent binding of HA protein. The surface analysis values were similar to those achieved in our previous studies, indicating that the synthesized DNA aptamer can be immobilized on the Au electrode properly.[23,36]

Detection of HA Protein in Buffer Solution. Figure 3a shows the I_D−V_G curves for bare Au electrode, immobilization of DNA aptamer, and HA protein binding. The resulting V_T shift of the extended-gate FET was related to the surface charge on the sensing electrode. A positive V_T shift after the immobilization of DNA aptamer on the extended-gate FET (Figure 3b) was caused due to negative charges on the DNA backbone.[37,38] In contrast, the binding of HA protein with the DNA aptamer resulted in a negative V_T shift (Figure 3b); this indicates that positive charges were induced on the extended-gate FET. As the concentration of the HA protein was increased, the I_D−V_G curves shifted to the left in parallel; this generated a more negative V_T shift (Figure 3c). As shown in Figure 3d, the measured data for the V_T shift could be expressed by the Sips model,[39,40] providing a generation of the Langmuir isotherms as $\Delta V_T = V_m \frac{(c/K_A)^a}{1+(c/K_A)^a}$, where c is the concentration of the HA protein, K_A is the equilibrium dissociation constant, V_m is the maximum signal with all binding sites occupied, and a is a characteristic parameter to present a distribution of binding energies. The best fit to the data for the HA protein in a buffer solution provides fitting parameters K_A = 169 pM, A = −180 mV, and a = 0.26. The V_T shift was linearly proportional to the log concentration of HA protein in a dynamic range of 10 pM to 10 nM (Figure 3d). The signal (20−140 mV) and limit of detection (~5.8 pM) of our sensor were comparable to or higher than those of other aptamer-based FET sensors.[24,25,27−29] However, direct comparisons could not be made due to different aptamer and target biomolecules. Various FET-based approaches have been proposed for AIV detection,[8−10,41−43] but this work is the first study to demonstrate the applicability of DNA aptamer as a bioreceptor, as summarized in Table I. The sensitivity and dynamic range of our sensor were compared to those of the previously reported FET-based sensors for AIV detection. A significantly high performance of our sensor could be achieved via a simple extended-gate approach based on a disposable sensing part and a reusable FET transducer; this is suitable for a low-cost diagnosis because expensive fabrication processes for nanoscale devices are dispensable.[13] Our aptamer-based FET sensor can also be applied to a chicken serum sample that is closer to a clinical condition as compared to a buffer solution; this will be discussed later.

The sensing mechanism for most of the FET-based biosensors involves an intrinsic charge of the target biomolecules, which is determined by their pI values.[44] When the pI value is lower (or higher) than the buffer pH, the target biomolecules develop a negative (or positive) charge. In particular, HA protein (pI value = 6.5) is negatively charged in the buffer solution (pH 7.4).[45] However, the negative charge of the HA protein cannot explain the negative V_T shift observed in the measurement (Figure 3d), which indicates the accumulation of positive charge on the sensing electrode. As an alternative to the intrinsic charge of the target biomolecule,[8,10,41−43] a conformational change of the DNA aptamer should be considered. Previous studies on DNA aptamers as receptors of FET sensors demonstrated that target-induced conformational changes of a DNA aptamer in proximity of an FET channel modulated the channel current.[28] As negatively charged DNA aptamers were reoriented away from the FET channel, "effective" positive charges were induced on the surface. Accordingly, we hypothesized that in the present study, the DNA aptamer with a negatively charged

https://dx.doi.org/10.1021/acs.analchem.0c00348
Anal. Chem. 2020, 92, 5524−5531

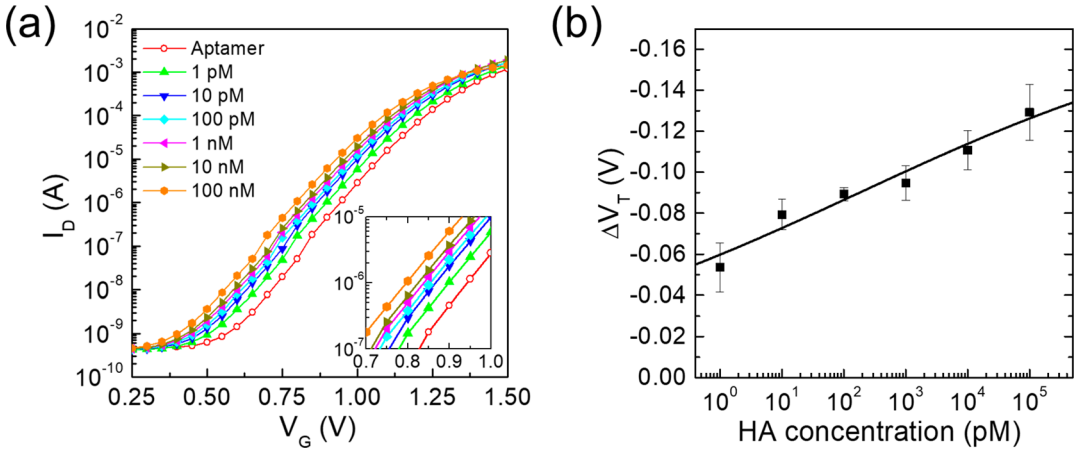

Figure 5. Detection of HA protein in a chicken serum sample. (a) I_D−V_G characteristics and (b) V_T shift of the aptamer-immobilized extended-gate FET with different concentrations of HA protein spiked in a chicken serum. The measured data are fit to the Sips model (solid line).

backbone moved away from the sensing electrode surface upon target capture, thereby increasing positive charges and decreasing V_T. Further research on conformational changes using fluorescence resonance energy transfer is required to comprehensively elucidate the exact underlying mechanisms.[28]

The DNA aptamer could be immobilized on the Au electrodes with different chemical linkers, such as cysteamine and 6-mercaptohexanoic acid, for functionalization (see Supporting Information). The magnitude of the signal at a given concentration of the HA protein was similar in both immobilization methods. However, the electrical stability under multiple gate sweeps was better in the direct immobilization of the DNA aptamer using thiol modification of the DNA end (Figure S4). In addition, this one-step modification allowed a simple, rapid, and low-cost fabrication of sensors.

Selectivity. A selectivity test of aptamer-functionalized sensors was conducted to examine the effect of nonspecific binding on the sensor characteristics. Figure 4 shows that other nonspecific proteins such as hemoglobin, BSA, and myoglobin generated a sensor signal; however, the observed value was less than that of the specific target (i.e., HA protein) in the same concentration. This type of the noise signal caused by nonspecific binding is typically observed in aptamer-based FET sensors.[29] The interference caused by nonspecific binding can be reduced by controlled passivation of the sensing electrodes outside the receptors.[27]

The V_T shift caused by nonspecific binding had a negative value, indicating the generation of a positive charge on the sensing surface. Because the nonspecific proteins were negatively charged in the neutral buffer solution (pH 7.4),[46−48] we speculate that a little conformational change in the aptamer occurred due to nonspecific binding. The binding-induced conformational change effectively suppressed the noise signal produced by a binding event itself, which generally occurs in electrochemical transduction through charge transfer on the surface. Despite using the same aptamer as the receptor, the FET-based sensor showed a lower noise level for nonspecific binding, compared to the electrochemical method.[23]

Detection of HA Protein in Chicken Serum. A chicken serum sample containing HA proteins was utilized to check the feasibility for on-site AI detection. As the concentration of the HA protein spiked in the chicken serum increases, the I_D−V_G curve was shifted to the left in parallel (Figure 5a). The direction of V_T shift in the serum (Figure 5b) was the same as that in the buffer solution (Figure 3d), confirming the same sensing mechanism. The measured data for the V_T shift were also fit to the Sips model[39,40] described in the previous section. We obtained the fitting parameters K_A = 178 pM, V_m = −180 mV, and a = 0.14. The dynamic range and limit of detection were 10 pM−10 nM and 5.9 pM, respectively. However, the sensitivity for HA detection degraded in the serum (12.4 mV/dec), compared to the buffer solution (26.7 mV/dec). The reduction in sensitivity was consistent with that in a previous study for detection of the malaria biomarker, where the complex nature in the serum medium hindered interaction between the aptamer and biomarker.[29] It is worth noting that the extrapolated signal at zero concentration is higher in the buffer solution. Other proteins, except for the target biomolecules, create nonspecific binding to achieve a noise signal, as already seen in Figure 4.

A lower ionic strength of the measurement buffer resulted in a higher sensing signal (Figure S5). This result is consistent with those of previous studies, where the effect of ionic strength on the signal of FET-based sensors was studied.[49,50] The charged biomolecules were screened using the dissolved solution counterions, which is called Debye screening.[51] Outside a certain characteristic length, termed the Debye length, the electric potential arising from the charged biomolecules decayed exponentially toward zero with an increase in distance.[49] The enlargement of Debye length using a buffer solution with lower ionic strength is a good way to increase the sensing signal. However, the diluted buffer solution may degrade the binding efficiency between the receptor and the target.[33] Short receptors within the Debye screening length are preferred to enhance the sensitivity in antibody-based receptors.[52] The special design of DNA aptamers to make a structural change to move into the Debye screening length is a strategy for overcoming the limitations of Debye length.[28]

CONCLUSIONS

We demonstrated the use of a label-free electrical biosensor based on a DNA aptamer-immobilized extended-gate FET to detect HA protein, a biomarker of H5N1 AIVs, in chicken serum. Its simple and low-cost architecture, based on a reusable FET transducer and disposable sensing part with

https://dx.doi.org/10.1021/acs.analchem.0c00348
Anal. Chem. 2020, 92, 5524−5531

direct immobilization of a sensitive and selective DNA aptamer, made it highly advantageous for biosensing. The multifunctional aptamer provided various functionalities, including target recognition, immobilization, and signal transduction. The aptamer-based FET biosensor could detect the target HA protein with a low detection limit of 5.8 pM in a wide detection range of 10 pM to 10 nM with a high sensitivity of 26.7 mV/dec in a buffer solution. Furthermore, the proposed FET biosensor was successfully applied for analysis of a diluted chicken serum sample to detect low concentrations of HA protein down to 5.9 pM in a wide linear range of 10 pM to 10 nM with sensitivity of 12.4 mV/dec, enabling the analysis in real samples. Probable mechanism underlying the observed negative V_T shift may be explained by reorientation of the negatively charged DNA aptamer away from the sensing electrode surface, which would increase the surface potential. The specificity of the biosensor was confirmed with relevant interfering proteins such as hemoglobin, BSA, and myoglobin. The aptamer is cheaper compared with other bioprobes that can pave the way for mass-production of AIV biosensors. Further integration of our aptamer-based FET biosensor with the microfluidic system and a portable readout circuit will offer rapid, easy-to-use, and portable detection to enable point-of-care diagnosis in real samples.

■ ASSOCIATED CONTENT

Supporting Information

The Supporting Information is available free of charge at https://pubs.acs.org/doi/10.1021/acs.analchem.0c00348.

Optical microscopy images of the sensing electrode, pH sensing characteristics of the extended-gate FET with SiO_2 layer, surface morphology of the sensing electrode, electrical stability depending on surface functionalization, and effect of Debye screening (PDF)

■ AUTHOR INFORMATION

Corresponding Authors

Taek Lee − *Department of Chemical Engineering, Kwangwoon University, Seoul 01897, Korea*; Email: tlee@kw.ac.kr

Jae-Hyuk Ahn − *Department of Electronic Engineering, Kwangwoon University, Seoul 01897, Korea*; orcid.org/0000-0001-7490-000X; Email: jaehahn@kw.ac.kr

Authors

Jae Kwon − *Department of Electronic Engineering, Kwangwoon University, Seoul 01897, Korea*

Yeonju Lee − *Department of Chemical Engineering, Kwangwoon University, Seoul 01897, Korea*

Complete contact information is available at: https://pubs.acs.org/10.1021/acs.analchem.0c00348

Author Contributions

[§]J.K. and Y.L. contributed equally to this work.

Notes

The authors declare no competing financial interest.

■ ACKNOWLEDGMENTS

This work was supported by the National Research Foundation of Korea (NRF) grant funded by the Korea government (MSIP; Ministry of Science, ICT & Future Planning) (No. 2017R1C1B5017451). J.-H.A. was partially supported by the Basic Science Research Program through the NRF grant funded by the Ministry of Education (No. 2018R1A6A1A03025242) and also by a Research Grant from the Kwangwoon University in 2019. T.L. was partially supported by the Basic Science Research Program through the NRF grant funded by the Ministry of Education (No. 2018R1D1A1B07049407) and also by a Research Grant from the Kwangwoon University in 2020.

■ REFERENCES

(1) Shortridge, K. F.; Zhou, N. N.; Guan, Y.; Gao, P.; Ito, T.; Kawaoka, Y.; Kodihalli, S.; Krauss, S.; Markwell, D.; Murti, K. G. *Virology* **1998**, *252* (2), 331−342.

(2) Claas, E. C.; Osterhaus, A. D.; Van Beek, R.; De Jong, J. C.; Rimmelzwaan, G. F.; Senne, D. A.; Krauss, S.; Shortridge, K. F.; Webster, R. G. *Lancet* **1998**, *351* (9101), 472−477.

(3) Subbarao, K.; Klimov, A.; Katz, J.; Regnery, H.; Lim, W.; Hall, H.; Perdue, M.; Swayne, D.; Bender, C.; Huang, J. *Science* **1998**, *279* (5349), 393−396.

(4) Sims, L.; Ellis, T.; Liu, K.; Dyrting, K.; Wong, H.; Peiris, M.; Guan, Y.; Shortridge, K. *Avian Dis.* **2003**, *47* (s3), 832−838.

(5) World Health Organization. Cumulative number of confirmed human cases of avian influenza A(H5N1) reported to WHO, 2003−2019. https://www.who.int/influenza/human_animal_interface/2019_06_24_tableH5N1.pdf (accessed on March 12, 2020).

(6) Spackman, E.; Senne, D. A.; Myers, T.; Bulaga, L. L.; Garber, L. P.; Perdue, M. L.; Lohman, K.; Daum, L. T.; Suarez, D. L. *J. Clin. Microbiol.* **2002**, *40* (9), 3256−3260.

(7) He, Q.; Velumani, S.; Du, Q.; Lim, C. W.; Ng, F. K.; Donis, R.; Kwang, J. *Clin. Vaccine Immunol.* **2007**, *14* (5), 617−623.

(8) Ahn, J.-H.; Choi, S.-J.; Han, J.-W.; Park, T. J.; Lee, S. Y.; Choi, Y.-K. *Nano Lett.* **2010**, *10* (8), 2934−2938.

(9) Ahn, J.-H.; Im, M.; Park, T. J.; Lee, S. Y.; Choi, Y.-K. *J. Biomed. Nanotechnol.* **2015**, *11* (9), 1640−1643.

(10) Park, S.; Choi, J.; Jeun, M.; Kim, Y.; Yuk, S. S.; Kim, S. K.; Song, C. S.; Lee, S.; Lee, K. H. *Adv. Healthcare Mater.* **2017**, *6* (13), 1700371.

(11) Cui, Y.; Wei, Q.; Park, H.; Lieber, C. M. *Science* **2001**, *293* (5533), 1289−1292.

(12) Stern, E.; Klemic, J. F.; Routenberg, D. A.; Wyrembak, P. N.; Turner-Evans, D. B.; Hamilton, A. D.; LaVan, D. A.; Fahmy, T. M.; Reed, M. A. *Nature* **2007**, *445* (7127), 519.

(13) Kwon, J.; Lee, B.-H.; Kim, S.-Y.; Park, J.-Y.; Bae, H.; Choi, Y.-K.; Ahn, J.-H. *ACS Sens* **2019**, *4* (6), 1724−1729.

(14) Park, K. S. *Biosens. Bioelectron.* **2018**, *102*, 179−188.

(15) Hong, K. L.; Sooter, L. J. *BioMed Res. Int.* **2015**, *2015*, 1.

(16) Pang, Y.; Rong, Z.; Wang, J.; Xiao, R.; Wang, S. *Biosens. Bioelectron.* **2015**, *66*, 527−532.

(17) Xu, L.; Wang, R.; Kelso, L. C.; Ying, Y.; Li, Y. *Sens. Actuators, B* **2016**, *234*, 98−108.

(18) Bai, H.; Wang, R.; Hargis, B.; Lu, H.; Li, Y. *Sensors* **2012**, *12* (9), 12506−12518.

(19) Nguyen, V.-T.; Seo, H. B.; Kim, B. C.; Kim, S. K.; Song, C.-S.; Gu, M. B. *Biosens. Bioelectron.* **2016**, *86*, 293−300.

(20) Lum, J.; Wang, R.; Lassiter, K.; Srinivasan, B.; Abi-Ghanem, D.; Berghman, L.; Hargis, B.; Tung, S.; Lu, H.; Li, Y. *Biosens. Bioelectron.* **2012**, *38* (1), 67−73.

(21) Lin, J.; Wang, R.; Jiao, P.; Li, Y.; Li, Y.; Liao, M.; Yu, Y.; Wang, M. *Biosens. Bioelectron.* **2015**, *67*, 546−552.

(22) Liu, X.; Cheng, Z.; Fan, H.; Ai, S.; Han, R. *Electrochim. Acta* **2011**, *56* (18), 6266−6270.

(23) Lee, T.; Park, S. Y.; Jang, H.; Kim, G.-H.; Lee, Y.; Park, C.; Mohammadniaei, M.; Lee, M.-H.; Min, J. *Mater. Sci. Eng., C* **2019**, *99*, 511−519.

(24) So, H.-M.; Won, K.; Kim, Y. H.; Kim, B.-K.; Ryu, B. H.; Na, P. S.; Kim, H.; Lee, J.-O. *J. Am. Chem. Soc.* **2005**, *127* (34), 11906−11907.

(25) Goda, T.; Miyahara, Y. *Biosens. Bioelectron.* **2012**, *32* (1), 244−249.

(26) Goda, T.; Miyahara, Y. *Biosens. Bioelectron.* **2013**, *45*, 89−94.
(27) Aliakbarinodehi, N.; Jolly, P.; Bhalla, N.; Miodek, A.; De Micheli, G.; Estrela, P.; Carrara, S. *Sci. Rep.* **2017**, *7*, 44409.
(28) Nakatsuka, N.; Yang, K.-A.; Abendroth, J. M.; Cheung, K. M.; Xu, X.; Yang, H.; Zhao, C.; Zhu, B.; Rim, Y. S.; Yang, Y. *Science* **2018**, *362* (6412), 319−324.
(29) Singh, N. K.; Thungon, P. D.; Estrela, P.; Goswami, P. *Biosens. Bioelectron.* **2019**, *123*, 30−35.
(30) Shiratori, I.; Akitomi, J.; Boltz, D. A.; Horii, K.; Furuichi, M.; Waga, I. *Biochem. Biophys. Res. Commun.* **2014**, *443* (1), 37−41.
(31) Ortiz-Conde, A.; Sánchez, F. G.; Liou, J. J.; Cerdeira, A.; Estrada, M.; Yue, Y. *Microelectron. Reliab.* **2002**, *42* (4−5), 583−596.
(32) *ICH Harmonised Tripartite Guideline: Validation of Analytical Procedures Methodology*; International Conference on Harmonization, 1996.
(33) Kim, A.; Ah, C. S.; Park, C. W.; Yang, J.-H.; Kim, T.; Ahn, C.-G.; Park, S. H.; Sung, G. Y. *Biosens. Bioelectron.* **2010**, *25* (7), 1767−1773.
(34) Chen, S.; Bomer, J. G.; Carlen, E. T.; van den Berg, A. *Nano Lett.* **2011**, *11* (6), 2334−2341.
(35) Tarasov, A.; Wipf, M.; Bedner, K.; Kurz, J.; Fu, W.; Guzenko, V.; Knopfmacher, O.; Stoop, R.; Calame, M.; Schönenberger, C. *Langmuir* **2012**, *28* (25), 9899−9905.
(36) Lee, T.; Lee, Y.; Park, S. Y.; Hong, K.; Kim, Y.; Park, C.; Chung, Y.-H.; Lee, M.-H.; Min, J. *Colloids Surf., B* **2019**, *175*, 343−350.
(37) Fritz, J.; Cooper, E. B.; Gaudet, S.; Sorger, P. K.; Manalis, S. R. *Proc. Natl. Acad. Sci. U. S. A.* **2002**, *99* (22), 14142−14146.
(38) Chen, C.-P.; Ganguly, A.; Lu, C.-Y.; Chen, T.-Y.; Kuo, C.-C.; Chen, R.-S.; Tu, W.-H.; Fischer, W. B.; Chen, K.-H.; Chen, L.-C. *Anal. Chem.* **2011**, *83* (6), 1938−1943.
(39) Sips, R. *J. Chem. Phys.* **1948**, *16* (5), 490−495.
(40) Ping, J.; Vishnubhotla, R.; Vrudhula, A.; Johnson, A. C. *ACS Nano* **2016**, *10* (9), 8700−8704.
(41) Gao, A.; Lu, N.; Dai, P.; Li, T.; Pei, H.; Gao, X.; Gong, Y.; Wang, Y.; Fan, C. *Nano Lett.* **2011**, *11* (9), 3974−3978.
(42) Hideshima, S.; Hinou, H.; Ebihara, D.; Sato, R.; Kuroiwa, S.; Nakanishi, T.; Nishimura, S.-I.; Osaka, T. *Anal. Chem.* **2013**, *85* (12), 5641−5644.
(43) Chan, C.; Shi, J.; Fan, Y.; Yang, M. *Sens. Actuators, B* **2017**, *251*, 927−933.
(44) Nair, P. R.; Alam, M. A. *IEEE Trans. Electron Devices* **2007**, *54* (12), 3400−3408.
(45) Di Lella, S.; Herrmann, A.; Mair, C. M. *Biophys. J.* **2016**, *110* (11), 2293−2301.
(46) Vigneshwaran, N.; Bijukumar, G.; Karmakar, N.; Anand, S.; Misra, A. In *Fluorescence and Biochemical Characterization of Glycated Hemoglobin*, Macromolecular Symposia; Wiley Online Library: 2003; pp 119−128.
(47) Vlasova, I.; Saletsky, A. *J. Appl. Spectrosc.* **2009**, *76* (4), 536−541.
(48) Graf, M.; García, R. G.; Wätzig, H. *Electrophoresis* **2005**, *26* (12), 2409−2417.
(49) Stern, E.; Wagner, R.; Sigworth, F. J.; Breaker, R.; Fahmy, T. M.; Reed, M. A. *Nano Lett.* **2007**, *7* (11), 3405−3409.
(50) Ping, J.; Xi, J.; Saven, J. G.; Liu, R.; Johnson, A. C. *Biosens. Bioelectron.* **2017**, *89*, 689−692.
(51) Hückel, E.; Debye, P. *Phys. Z.* **1923**, *24*, 185−206.
(52) Kim, J. P.; Lee, B. Y.; Hong, S.; Sim, S. J. *Anal. Biochem.* **2008**, *381* (2), 193−198.

https://dx.doi.org/10.1021/acs.analchem.0c00348
Anal. Chem. 2020, 92, 5524−5531